

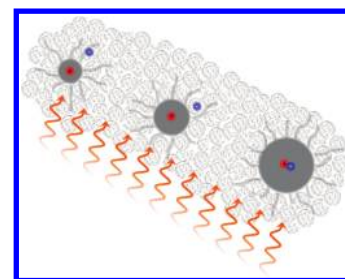
# Size-Dependent Electron Transfer from Colloidal PbS Nanocrystals to Fullerene

Agnieszka Gocalińska,<sup>†</sup> Michele Saba,<sup>\*†</sup> Francesco Quochi,<sup>†</sup> Marco Marceddu,<sup>†</sup> Krisztina Szendrei,<sup>‡</sup> Jia Gao,<sup>‡</sup> Maria A. Loi,<sup>‡</sup> Maksym Yarema,<sup>§</sup> Robert Seyrkammer,<sup>§</sup> Wolfgang Heiss,<sup>§</sup> Andrea Mura,<sup>†</sup> and Giovanni Bongiovanni<sup>†</sup>

<sup>†</sup>Dipartimento di Fisica and SLACS-CNR/INFN, Università di Cagliari, I-09042 Monserrato, Italy, <sup>‡</sup>Zernike Institute for Advanced Materials, University of Groningen, Groningen, 9747 AG, The Netherlands, and <sup>§</sup>Institute of Semiconductor and Solid State Physics, Johannes Kepler University, Austria

**ABSTRACT** We investigate a promising organic/inorganic hybrid composite for solution-processable optoelectronics made by lead sulphide nanoparticles and fullerene derivatives, which combine the sensitivity of PbS to the infrared spectrum with the good electron transport properties of fullerenes. Charge separation is the crucial process that determines whether the heterojunction can be the building block for devices converting photogenerated excitons into free charges flowing in a circuit. Subpicosecond spectroscopy techniques on bulk heterojunctions between PbS nanocrystals of various sizes and [6,6]-phenyl-61-butyrac acid methyl ester (PCBM) were employed to reveal the ultrafast dynamics of photoexcited carriers, particularly transfer of photoexcited electrons from nanocrystals to PCBM. Electron transfer is found to critically depend on nanoparticle size, occurring for nanocrystals with diameter 4.4 nm and smaller, not for larger ones. Our findings are relevant to the engineering of hybrid solar cells and light detectors based on PbS nanocrystal/fullerene bulk heterojunctions.

**SECTION** Nanoparticles and Nanostructures



Colloidal semiconductor nanocrystals have attracted wide interest during recent years because of their easy solution synthesis and processability,<sup>1</sup> size-dependent optical properties,<sup>2</sup> and wide scope of applications, ranging from biology to electronics, including photosensing and photovoltaic devices.<sup>3–7</sup> Optical properties of nanocrystals can be easily determined and controlled during synthesis, but the functionality of optoelectronic devices also critically depends on electric conduction in nanocrystal films, which typically occurs by hopping through surfactants that separate nanocrystals and is much more difficult to control and optimize. Semiconductor nanocrystals blended with organic semiconductors form a novel class of hybrid materials for optoelectronics with the potential for improved charge transport properties as well as extended and tailorable functionalities. A promising hybrid composite is made by lead sulphide nanocrystals and fullerene derivatives, which benefits from the sensitivity of PbS to the infrared spectrum, the potential for carrier multiplication<sup>8–10</sup> and the good electron transport properties of fullerenes.<sup>11</sup> The size-dependent band gap of nanocrystals offers the opportunity of controlling the energy level alignment with respect to fullerene, which ultimately determines the possibility of free charge generation at the heterojunction following optical excitation. Successful fabrication of infrared light detectors and imagers based on blends containing PbS nanocrystals were demonstrated.<sup>12,13</sup>

Semiconductor heterojunctions are classified according to the relative alignment of the electron affinity (EA) and ionization potential (IP) of the two materials. In a type I heterojunction, the band edges of a semiconductor fall within the energy gap of the second one, while a type II heterojunction is formed when a staggered level alignment sets in (Figure 1a). Only in this latter case is charge separation at the junction interface energetically favorable, and thus the junction may serve to convert photogenerated excitons into free charge carriers. PbS nanocrystals and fullerenes can in principle form both kinds of heterojunction. Fullerene derivative bandgaps depend on the exact chemical composition and can be tuned with the addition of an organic tail, whose primary role is to increase the solubility. In particular, [6,6]-phenyl-61-butyrac acid methyl ester (PCBM) lowest unoccupied molecular orbital (LUMO) is usually reported between  $-4.2$  eV<sup>14,15</sup> and  $-4.3$  eV,<sup>16,17</sup> although values as high as  $-3.7$  eV have been sometimes assumed.<sup>18,19</sup> The bandgap of bulk PbS is 0.41 eV with EA around  $-4.6$  eV and IP of  $-5.0$  eV.<sup>20</sup> Quantum confinement energy in nanocrystals can increase the optical bandgap up to  $\sim 1.5$  eV, shifting the EA above the LUMO level of PCBM.<sup>21</sup> When considering hybrid heterojunctions between PbS nanocrystals and PCBM, there

**Received Date:** January 28, 2010

**Accepted Date:** March 12, 2010

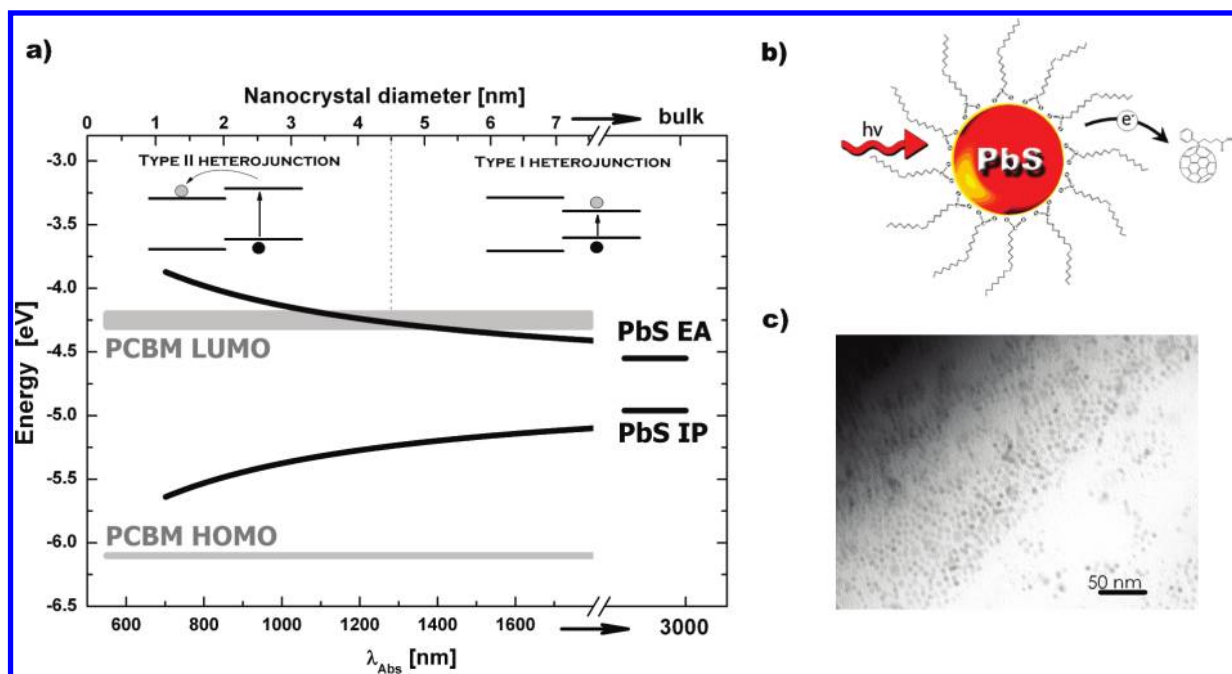


**Figure 1.** (a) Sketch of energy level alignment at the PbS nanocrystal/PCBM interface. IP and EA levels of PbS nanocrystals were calculated from the optical bandgap as described in the text<sup>29</sup> ( $\lambda_{\text{Abs}}$  represented the wavelength of the first excitonic absorption maximum of PbS nanocrystals). (b) Sketch of hybrid heterojunction with graphical representation of photoinduced electron transfer from PbS nanocrystal to PCBM molecule. (c) TEM image of a nanocrystal/PCBM blend drop cast on an electron microscope carbon grid. PbS nanocrystals were seen immersed into a PCBM layer.

exists therefore a critical size for PbS nanocrystals for which a transition occurs from type I to type II heterojunction. The absolute positions of conduction and valence bands for nanocrystals depend not only on materials, but also on size,<sup>2</sup> shape<sup>22</sup> and capping agents,<sup>23</sup> with some of these effects difficult to model theoretically with the necessary accuracy to reliably estimate the level crossing; recent reports have even questioned the very existence of band crossing.<sup>19</sup> The critical nanocrystal size and emission wavelength below which charge separation takes place is extremely relevant to optoelectronic applications in the near-infrared spectral region and deserve a direct experimental assessment. The knowledge of the electron transfer dynamics at the PCBM/nanocrystal interface and its competition with multiexciton annihilation processes are also significant for the exploitation of carrier multiplication<sup>9</sup> in nanocrystal composites.

In this work, we investigated bulk heterojunctions between PbS nanocrystals of various sizes and PCBM (Figure 1b and 1c). Subpicosecond spectroscopy techniques on blends were employed to reveal the ultrafast dynamics of photoexcited carriers at the heterojunction, particularly transfer of photoexcited electrons from nanocrystals to PCBM.

Colloidal PbS nanocrystals of various sizes capped with oleic acid were synthesized by known methods<sup>24</sup> and characterized by optical spectroscopy, showing the first exciton peak in the absorption spectrum at 1010, 1110, 1150, 1250, and 1350 nm (Figure 2). In order to estimate the nanocrystal diameter, we used the calibration relationship between the first excitonic peak position and the nanocrystal size from the transmission electron microscopy (TEM) measurements reported in ref 25. Accordingly, absorption maxima of our

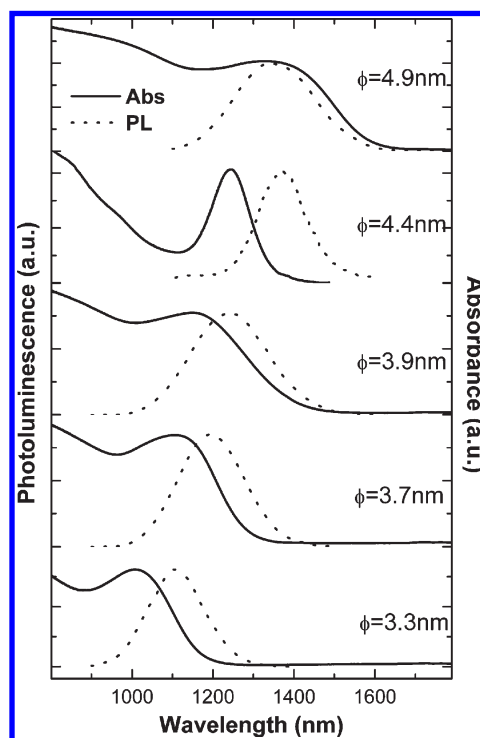


**Figure 2.** Normalized absorbance (solid line) and photoluminescence (dash line) spectra of PbS nanocrystals of five different diameters. Vertical offsets are for clarity. Photoluminescence spectra were measured in air; therefore the spectrum for 4.9 nm nanocrystals could have been distorted by the water absorption line around 1470 nm.

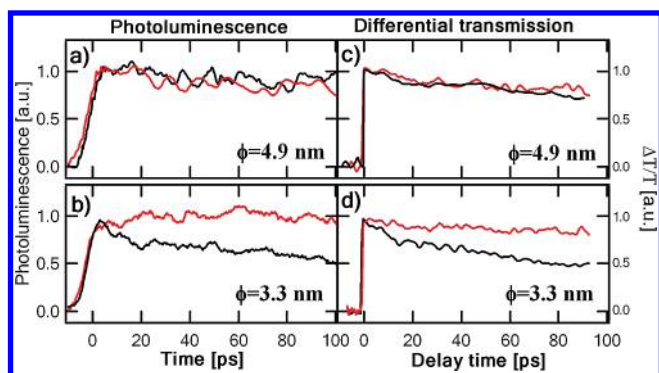


**Figure 3.** (a,b) Normalized time-resolved photoluminescence decays for pure nanocrystals (red lines) and blends with PCBM (black lines) of PbS nanocrystals with diameters  $\phi = 4.9$  and  $3.3$  nm. (c,d) Decay of the differential transmission signal as a function of the pump–probe delay for pure nanocrystals (red lines) and blends with PCBM (black lines) of PbS nanocrystals with diameters  $\phi = 4.9$  and  $3.3$  nm.

nanocrystals corresponded to nanocrystal diameters of 3.3, 3.7, 3.9, 4.4, and 4.9 nm, respectively, covering an interesting size range where a transition between type I and type II alignment with PCBM energy levels was expected. Solution blends were prepared with an excess of PCBM in volume and then drop cast on a glass slide to form bulk heterojunctions. TEM images (Figure 1c) confirmed that a considerable fraction of nanocrystals were embedded in a PCBM matrix and did not cluster. Morphology was a crucial feature to be able to probe the heterojunction at the molecular scale. Having isolated nanocrystals in a PCBM matrix allowed us to decouple the charge splitting process taking place at the PbS/PCBM molecular interface from more complex phenomena involving exciton hopping within nanocrystal clusters. Films of unblended nanocrystals served as a reference.

Time-resolved optical spectroscopy experiments were performed to determine the dependence of the electron transfer time on nanocrystal diameter. PbS nanocrystals were excited with 150 fs-long laser pulses, 800 nm in wavelength, with sub-nanojoule pulse energies and repetition rates adjustable from 80 MHz to several kilohertz. Photoluminescence was spectrally and then temporally resolved with an infrared-sensitive streak camera. The photoluminescence decays presented in Figure 3a,b were measured for films of pure nanocrystals and nanocrystal/PCBM blends prepared with nanocrystals having the largest and smallest sizes,  $\phi = 4.9$  and  $3.3$  nm, respectively. While for the largest diameter the photoluminescence decay was very similar for pure and blend films (a single exponential fit to the data gave  $\tau \sim 40$  ns as the characteristic time; see the Supporting Information for details), the photoluminescence for the smallest nanocrystals from the blend decayed much faster than the reference pure nanocrystal film ( $\tau = 170$  ps vs 75 ns). At long delays after excitation, the decay time became slower. While the early decay of the photoluminescence was independent of thin film preparation conditions, the intensity of the long-lasting tail was quite sensitive on the procedure used to deposit the film. (Longer time-scale photoluminescence decays have been included in the Supporting Information).

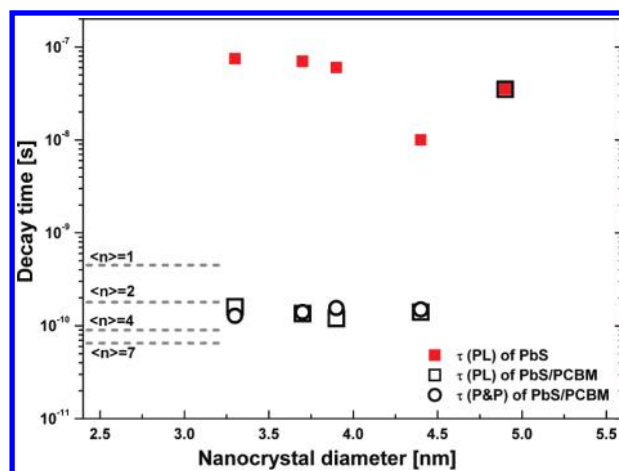


**Figure 4.** Photoluminescence (square markers) and transient absorption (circle markers) decay times as a function of nanocrystal diameter for blends (black markers) and pure nanocrystal films (red markers). The dashed lines mark the multiexciton lifetimes for excitation levels creating an average number of  $\langle n \rangle$  excitons per nanocrystal as estimated through transient absorption measurements (details in the Supporting Information). With our transient absorption setup we could only estimate decays shorter than 1 ns because of the limited range of the topical delay line. Points corresponding to transient absorption decays longer than 1 ns were therefore not included in the plot.

To detect possible faster decay transients, photoluminescence measurements were complemented by femtosecond transmission experiments, which allowed for a much shorter, subpicosecond time resolution. Laser pulses, 150 fs-long, 1 kHz repetition rate, were provided by a regenerative amplifier; the pump wavelength (784 nm) was chosen to excite predominantly nanocrystals and not fullerene molecules. Pump intensity was kept low enough that each pulse created on average less than 1 exciton per nanocrystal (a typical excitation level was 0.2 excitons per pulse in each nanocrystal; incidentally, the pump photon energy was too low for carrier multiplication to occur, therefore no multiexcitons were created in the linear regime). Differential transmission<sup>26</sup> of probe pulses resonant with the exciton transition was recorded as a function of the pump–probe delay. The dynamics of differential transmission (Figure 3c,d) proved to be similar to what was observed in luminescence, with a faster decay in blend films than in pure nanocrystal films for small nanocrystals ( $\phi = 3.3$  nm), while the decay was not affected by the presence of PCBM for larger nanocrystals ( $\phi = 4.9$  nm).

A systematic investigation over various nanocrystal sizes was carried out by repeating the photoluminescence and pump–probe experiments for nanocrystals of intermediate sizes,  $\phi = 3.7, 3.9,$  and  $4.4$  nm. As summarized in Figure 4, a single exponential fit to the decay to the photoluminescence from pure PbS thin films gave characteristic times of 40, 10, 65, 70, and 75 ns ( $\pm 10$  ns) for samples with  $\phi = 4.9, 4.4, 3.9, 3.7,$  and  $3.3$  nm, respectively (decay times were much longer for nanocrystals in solution, as shown in the Supporting Information). The decay of nanocrystal emission in blends was shortened to less than 1 ns for nanocrystal sizes equal or smaller than 4.4 nm (single exponential fits in the temporal

window 0–100 ps to the data gave  $\tau = 140 \text{ ps} \pm 20 \text{ ps}$  (statistical error for sizes  $\phi = 4.4, 3.9, 3.7,$  and  $3.3 \text{ nm}$ ), while the decay for the blend with nanocrystals of  $\phi = 4.9 \text{ nm}$  was hardly distinguishable from the one for a pure PbS thin film. Analogously, we observed significantly faster decays of the differential transmission signal with respect to the probe delay in drop cast films of PbS/PCBM containing nanocrystals with diameter  $\phi = 4.4, 3.9, 3.7,$  and  $3.3 \text{ nm}$  (approximately  $\tau = 150 \text{ ps}$  could be estimated for all these decays within a statistical uncertainty of  $\pm 15 \text{ ps}$ ) than in the sample with nanocrystals  $\phi = 4.9 \text{ nm}$ . Differential transmission spectra of pure nanocrystals of all diameters and PCBM/PbS nanocrystals  $\phi = 4.9 \text{ nm}$  were similar and did not show considerable decay in our scanning range. Overall, all blends except for the one with largest nanocrystals ( $\phi = 4.9 \text{ nm}$ ) showed decay times for both photoluminescence and differential transmission much faster than the corresponding reference pure nanocrystal films.

The shorter lifetime of both photoluminescence and differential transmission signal at the exciton resonance could be attributed to electron transfer from a PbS nanocrystal to a nearby PCBM molecule.<sup>12,27,28</sup> We could speculate that the slowing down of the photoluminescence decay observed at longer delays was due to the decay of the excitations created in nanocrystal clusters. The larger the aggregate, the longer the time excitons took to find a PCBM molecule where they may split. This interpretation was corroborated by the fact that the intensity of the long-lasting tail depended on sample preparation, which could influence nanocrystal aggregation (in all instances, the amplitude of the signal generated by long-living nanocrystals was less than 1 % of the total photoluminescence signal).

Time-resolved spectroscopy data indicated that electron transfer to the acceptor molecule occurred for blends with nanocrystal diameters equal to or smaller than  $\phi = 4.4 \text{ nm}$ , while it did not occur for nanocrystals with diameter  $\phi = 4.9 \text{ nm}$ . Uncertainties in the determination of nanocrystal size threshold were expected from homogeneous and inhomogeneous linewidths in both nanocrystal and PCBM energy levels. We estimated that, for all samples investigated, the dominant contribution to energy linewidths was the  $\sim 70 \text{ meV}$  (full width at half-maximum (fwhm)) of inhomogeneous broadening related to the nanocrystal size dispersion, exceeding homogeneous broadening ( $k_B T \sim 26 \text{ meV}$ ).

This experimental finding appeared consistent with the sketch shown in Figure 1a, where level crossing occurred for nanocrystals of diameter  $\phi = (4.25 \pm 0.75) \text{ nm}$  (with first excitonic peak maximum around  $\sim 1300 \text{ nm}$ ). The dependence of EA on nanocrystal size was calculated within a rather crude approximation,<sup>29</sup> in which several phenomena influencing electronic level positions with respect to the vacuum level were neglected, e.g., electron–hole interaction (which should, however, account for  $\sim 10 \text{ meV}$ ),<sup>30</sup> band dispersion and mixing, electrostatic effects, and interface dipole. The present experimental estimation of the critical nanocrystal diameter for electron transfer to occur could thus serve to validate accurate microscopic models addressing the issue of electronic level alignment in the PCBM/nanocrystal heterojunction at the molecular scale.

One could also expect that the time required for electrons to be transferred from nanocrystals to PCBM would depend on the energy jump between levels in the two materials. Results in Figure 4 indicated that for blends with nanocrystal sizes ranging from 3.3 to 4.4 nm there was no significant variation of photoluminescence or differential transmission signal decays as a function of nanocrystal size. This implied that, in the limited range we could explore, the electron transfer time was not clearly influenced by the nanocrystal diameter, provided that nanocrystals were small enough for charge transfer to occur. Similar results were reported for the electron transfer time from colloidal PbS nanocrystals into  $\text{TiO}_2$  nanoparticles.<sup>31</sup> On the other hand, in CdSe nanocrystals linked to mesoporous  $\text{TiO}_2$  electron transfer time was size-dependent, ranging from  $\sim 100 \text{ ps}$  to several tens of nanoseconds<sup>28</sup> for varying energy difference between the acceptor and donor levels. In the PbS/PCBM composite, the change of the EA level for similar variation of the nanocrystal size can be easily calculated assuming equal electron and hole PbS masses<sup>32</sup> and equates half the energy gap variation, i.e.,  $\sim 110 \text{ meV}$ , but no increase of the transfer time was observed. A microscopic theory should model in a realistic way the donor/acceptor interface to understand which interactions precluded a faster electron extraction from smaller nanocrystal sizes. A comprehensive understanding should also account for capping agents, oleic acid molecules in our samples, which are expected to provide a barrier for electron transfer and bear influence on absolute values and size-dependent trends of electron transfer times.

Also shown in Figure 4, the measured electron transfer time was shorter than Auger recombination time for pump power even exceeding two excitons per nanocrystal on average<sup>33</sup> (see Supporting Information for details). This effect may enhance the efficiency of short wavelength photon-to-electron conversion in photodetector<sup>10</sup> and photovoltaic devices<sup>4</sup> by exploiting the process of carrier multiplication.<sup>8,9</sup>

Photocurrent measurements on nanocrystal/PCBM films drop cast on  $20 \mu\text{m}$ -spacing interdigitated electrodes demonstrated that photoelectrons transferred from nanocrystals to PCBM were indeed available for electrical conduction. Responsivity spectra, measured under monochromatic tunable illumination, are shown in Figure 5 for blends with nanocrystals in three different sizes. Responsivity extended as far in the infrared range as nanocrystal absorption spectra, proving that the blends were activated by photoexcitations of nanocrystals and not of PCBM. The photocurrent response was at least 2 orders of magnitude higher for blends containing  $\phi = 3.0 \text{ nm}$  nanocrystals than for the ones with  $\phi = 4.9$  and  $8.0 \text{ nm}$  nanocrystals. As photocurrent was activated by charge separation, measurements in Figure 5 were a confirmation that charge transfer occurred only for nanocrystals smaller than  $4.9 \text{ nm}$ . The photocurrent for blends with  $\phi = 4.9 \text{ nm}$  nanocrystals did not peak in correspondence with the first exciton transition of nanocrystals, but at shorter wavelength, an effect that could be due to a remnant subset of smaller nanocrystals in the blend for which charge transfer occurred. Current–voltage characteristics of measured samples are included in the Supporting Information (Figure S5).

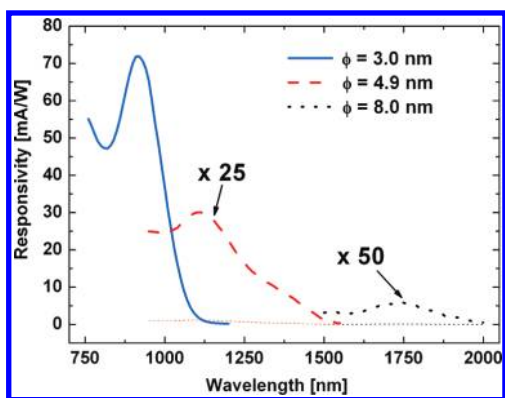


**Figure 5.** Responsivity spectra of PbS/PCBM thin films under CW excitation measured at 100 V bias for PbS/PCBM blends with nanocrystals smaller than transfer threshold ( $\phi = 3.0$  nm, solid blue line) and larger than the threshold ( $\phi = 4.9$  nm - red dashed line;  $\phi = 8.0$  nm - black dotted line).

In conclusion, we were able to demonstrate that electron transfer from PbS nanocrystals to PCBM fullerene is tunable with nanocrystal size. The crossing between transferring and nontransferring junctions occurred for nanocrystals with optical transitions in the very useful near-infrared range, around 1300 nm in wavelength. For nanocrystals with shorter emission wavelength, electron transfer time was around 130–150 ps, fast enough to compete with recombination processes detrimental for the exploitation of carrier multiplication processes in PbS. Information we gathered may prove crucial to the development of hybrid photodetectors and solar cells exploiting absorption of nanocrystals to harvest infrared and near-UV solar emission.

**SUPPORTING INFORMATION AVAILABLE** Experimental details. Transient absorption data not shown in the main text (pure nanocrystal films and blends with  $\phi = 3.7$ , 3.9, and 4.4 nm); transient absorption as a function of pump excitation density (pure nanocrystals,  $\phi = 3.3$  nm); differential transmission spectrogram of PbS  $\phi = 3.3$  nm/PCBM thin film; photoluminescence decays of solutions and thin films of PbS and PbS/PCBM; current–voltage characteristics of thin films of PbS and PbS/PCBM blends with nanocrystals  $\phi = 3.0$ , 4.9, and 8.0 nm drop-cast on interdigitated electrodes. This material is available free of charge via the Internet at <http://pubs.acs.org>.

## AUTHOR INFORMATION

### Corresponding Author:

\*To whom correspondence should be addressed. E-mail: [michele.saba@dsf.unica.it](mailto:michele.saba@dsf.unica.it); phone: 0039 070 675 4872.

**ACKNOWLEDGMENT** This work was supported by the European Commission through the Human Potential Programme (Marie-Curie RTN NANOMATCH, Grant No. MRTN-CT-2006-035884), by the Italian Ministero dell'Istruzione dell'Università e della Ricerca through Grants FIRB-MIUR (project Synergy-FIRBRBNE03S7XZ) and 'Rientro dei cervelli', by the Italian National Research Council (CNR) with an INFM-CNR (Seed project for young researchers) and by the Austrian Science Fund (FWF, projects SFB IRON and START Y179).

## REFERENCES

- (1) Yin, Y.; Alivisatos, A. P. Colloidal Nanocrystal Synthesis and the Organic–Inorganic Interface. *Nature* **2005**, *437*, 664–670.
- (2) Alivisatos, A. P. Semiconductor Clusters, Nanocrystals, and Quantum Dots. *Science* **1996**, *271*, 933–937.
- (3) Konstantatos, G.; Howard, I.; Fischer, A.; Hoogland, S.; Clifford, J.; Klem, E.; Levina, L.; Sargent, E. H. Ultrasensitive Solution-Cast Quantum Dot Photodetectors. *Nature* **2006**, *442*, 180–183.
- (4) Nozik, A. J. Quantum Dot Solar Cells. *Physica E* **2002**, *14*, 115–120.
- (5) Plass, R.; Pelet, S.; Krueger, J.; Gratzel, M. Thiol-Capping of CdTe Nanocrystals: An Alternative to Organometallic Synthetic Routes. *J. Phys. Chem. B* **2002**, *106*, 7578–7585.
- (6) McDonald, S. A.; Konstantatos, G.; Zhang, S.; Cyr, P. W.; Klem, E. J. D.; Levina, L.; Sargent, E. H. Solution-Processed PbS Quantum Dot Infrared Photodetectors and Photovoltaics. *Nat. Mater.* **2005**, *4*, 138–142.
- (7) Böberl, M.; Kovalenko, M. V.; Gamerith, S.; List, E. J. W.; Heiss, W. Inkjet-Printed Nanocrystal Photodetectors Operating up to 3  $\mu$ m Wavelengths. *Adv. Mater.* **2007**, *19*, 3574–3578.
- (8) McGuire, J. A.; Joo, J.; Pietryga, J. M.; Schaller, R. D.; Klimov, V. I. New Aspects of Carrier Multiplication in Semiconductor Nanocrystals. *Acc. Chem. Res.* **2008**, *41*, 1810–1819.
- (9) Beard, M. C.; Midgett, A. G.; Law, M.; Semonin, O. E.; Ellingson, R. J.; Nozik, A. J. Variations in the Quantum Efficiency of Multiple Exciton Generation for a Series of Chemically Treated PbSe Nanocrystal Films. *Nano Lett.* **2009**, *9*, 836–845.
- (10) Sukhovatkin, V.; Hinds, S.; Brzozowski, L.; Sargent, E. H. Colloidal Quantum-Dot Photodetectors Exploiting Multiexciton Generation. *Science* **2009**, *324*, 1542–1544.
- (11) Mihailetchi, V. D.; van Duren, J. K. J.; Blom, P. W. M.; Hummelen, J. C.; Janssen, R. A. J.; Kroon, J. M.; Rispens, M. T.; Verhees, W. J. H.; Wienk, M. M. Electron Transport in a Methanofullerene. *Adv. Funct. Mater.* **2003**, *13*, 43–46.
- (12) Szendrei, K.; Cordella, F.; Kovalenko, M. V.; Böberl, M.; Hesser, G.; Yarema, M.; Jarzab, D.; Mikhnenko, O. V.; Gocalinska, A.; Saba, M.; et al. Solution-Processable Near-IR Photodetectors Based on Electron Transfer from PbS Nanocrystals to Fullerene Derivatives. *Adv. Mater.* **2009**, *21*, 683–687.
- (13) Rauch, T.; Böberl, M.; Tedde, S. F.; Fürst, J.; Kovalenko, M. V.; Hesser, G.; Lemmer, U.; Heiss, W.; Hayden, O. Near-Infrared Imaging with Quantum-Dot-Sensitized Organic Photodiodes. *Nat. Photonics* **2009**, *3*, 332–336.
- (14) Brabec, C. J.; Craviano, A.; Meissner, D.; Sariciftci, N. S.; Fromherz, T.; Rispens, M. T.; Sanchez, L.; Hummelen, J. C. Origin of the Open Circuit Voltage of Plastic Solar Cells. *Adv. Funct. Mater.* **2001**, *11*, 374–380.
- (15) Gong, X.; Tong, M.; Xia, Y.; Cai, W.; Moon, J. S.; Cao, Y.; Yu, G.; Shieh, C.-L.; Nilsson, B.; Heeger, A. J. High-Detectivity Polymer Photodetectors With Spectral Response from 300 nm to 1450 nm. *Science* **2009**, *325*, 1665–1667.
- (16) Scharber, M. C.; Mühlbacher, D.; Koppe, M.; Denk, P.; Waldauf, Ch.; Heeger, A. J.; Brabec, Ch. J. Design Rules for Donors in Bulk-Heterojunction Solar Cells—Towards 10% Energy-Conversion Efficiency. *Adv. Mater.* **2006**, *18*, 789–794.
- (17) Kim, J. Y.; Lee, K.; Coates, N. E.; Moses, D.; Nguyen, T.-Q.; Dante, M.; Heeger, A. J. Efficient Tandem Polymer Solar Cells Fabricated by All-Solution Processing. *Science* **2007**, *317*, 222–225.
- (18) Lee, T. W.; Byun, Y.; Koo, B. W.; Kang, I.-N.; Lyu, Y. Y.; Lee, C. H.; Pu, L.; Lee, S. Y. All-Solution-Processed n-Type Organic

- Transistors Using a Spinning Metal Process. *Adv. Mater.* **2005**, *17*, 2180–2184.
- (19) Dissanayake, D. M. N. M.; Lutz, T.; Curry, R. J.; Silva, S. R. P. Measurement and Validation of PbS-Nanocrystal Energy Levels. *Appl. Phys. Lett.* **2008**, *93*, 043501.
- (20) Brütting, W. *Physics of Organic Semiconductors Handbook*; Wiley-VCH, 2005.
- (21) Brus, L. E. A Simple Model for the Ionization Potential, Electron Affinity, and Aqueous Redox Potentials of Small Semiconductor Crystallites. *J. Chem. Phys.* **1983**, *79*, 5566–5571.
- (22) Hens, Z.; Vanmaekelbergh, D.; Stoffels, E. J. A. J.; van Kempen, H. Effects of Crystal Shape on the Energy Levels of Zero-Dimensional PbS Quantum Dots. *Phys. Rev. Lett.* **2002**, *88*, 236803.
- (23) Soreni-Harari, M.; Yaacobi, N.; Steiner, D.; Aharoni, A.; Banin, U.; Millo, O.; Tessler, N. Tuning Energetic Levels in Nanocrystal Quantum Dots through Surface Manipulations. *Nano Lett.* **2008**, *8*, 678–684.
- (24) Hines, M. A.; Scholes, G. D. Colloidal PbS Nanocrystals with Size-Tunable Near-Infrared Emission: Observation of Post-Synthesis Self-Narrowing of the Particle Size Distribution. *Adv. Mater.* **2003**, *21*, 1844–1849.
- (25) Moreels, I.; Lambert, K.; Smeets, D.; De Muynck, D.; Nollet, T.; Martins, J. C.; Vanhaecke, F.; Vantomme, A.; Delerue, Ch.; Allan, G.; Hens, Z. Size-Dependent Optical Properties of Colloidal PbS Quantum Dots. *ACS Nano* **2009**, *3*, 3023–3030.
- (26) Differential absorption  $\Delta A$  can be calculated from measured differential transmission  $\Delta T$  neglecting reflection, through the relation  $A = 1 - T$ , implying  $\Delta A = -\Delta T$ .
- (27) Kang, I.; Wise, F. W. Electronic Structure and Optical Properties of PbS and PbSe Quantum Dots. *J. Opt. Soc. Am. B* **1997**, *14*, 1632–1646.
- (28) Robel, I.; Kuno, M.; Kamat, P. V. Size-Dependent Electron Injection from Excited CdSe Quantum Dots into TiO<sub>2</sub> Nanoparticles. *J. Am. Chem. Soc.* **2007**, *129*, 4136–4137.
- (29) EA and IP of nanocrystals (EA<sub>NC</sub>, IP<sub>NC</sub>) were calculated using the formula  $EA_{NC} = EA_{bulk} + [m_{electron}^*(E_{NC}^g - E_{bulk}^g)] / (m_{electron}^* + m_{hole}^*)$   $IP_{NC} = IP_{bulk} - [m_{hole}^*(E_{NC}^g - E_{bulk}^g)] / (m_{electron}^* + m_{hole}^*)$ , where  $E_{NC,bulk}^g$  are the band gap energies for nanocrystal and bulk semiconductor, and  $m_{electron,hole}^*$  are effective masses of charges. We used equal effective masses for electron and hole in PbS.
- (30) Klimov, V. I. *Semiconductor and Metal Nanocrystals*; Marcel Dekker, Inc., 2004.
- (31) Hyun, B.-R.; Zhong, Y.-W.; Bartnik, A. C.; Sun, L.; Abruna, H. D.; Wise, F. W.; Goodreau, J. D.; Matthews, J. R.; Leslie, T. M.; Borrelli, N. F. Electron Injection from Colloidal PbS Quantum Dots into Titanium Dioxide Nanoparticles. *ACS Nano* **2008**, *2*, 2206–2212.
- (32) Baskoutas, S.; Terzis, A. F. Size Dependent Exciton Energy of Various Technologically Important Colloidal Quantum Dots. *Mater. Sci. Eng., B* **2008**, *147*, 280–283.
- (33) Istrate, E.; Hoogland, S.; Sukhovatkin, V.; Levina, L.; Myrskog, S.; Smith, P. W. E.; Sargent, E. H. Carrier Relaxation Dynamics in Lead Sulfide Colloidal Quantum Dots. *J. Phys. Chem. B* **2008**, *112*, 2757–2760.